

On the Possibility of a Strong First-Order Phase Transition in Neutron Stars

ZHENG CAO ^{1,2} AND LIE-WEN CHEN ¹

¹*State Key Laboratory of Dark Matter Physics, Key Laboratory for Particle Astrophysics and Cosmology (MOE), and Shanghai Key Laboratory for Particle Physics and Cosmology, School of Physics and Astronomy, Shanghai Jiao Tong University, Shanghai 200240, China*

²*Tsung-Dao Lee Institute, Shanghai Jiao Tong University, Shanghai 201210, China*

ABSTRACT

Whether cold dense QCD matter undergoes a strong first-order phase transition remains an open question. In nature, neutron stars provide the most direct probe of cold dense QCD matter. Theoretically, chiral effective field theory constrains the equation of state of dense matter near nuclear saturation density, while perturbative QCD calculations constrain it at densities well beyond stable neutron-star interiors. We perform Bayesian inference with non-parametric Gaussian-process equation of state for β -equilibrated neutron-star matter under the assumption with and without a strong first-order phase transition, using the tidal deformability from GW170817, the NICER mass–radius measurements of PSR J0740+6620, PSR J0030+0451, PSR J0437–4715, PSR J0614–3329, chiral effective field theory, and perturbative QCD. Our results favor a strong first-order phase transition, with its onset most likely lying *above* the central density of the most massive neutron star. Such an onset reconciles the stiffness required to support massive neutron stars with the softening favored by perturbative QCD from asymptotically high density.

Keywords: Neutron stars (1108) — Nuclear astrophysics (1129) — Nuclear physics (2077)

1. INTRODUCTION

The phase structure of strong interaction matter at several times nuclear saturation density, $n_0 \equiv 0.16 \text{ fm}^{-3}$, remains a central open problem in nuclear physics and astrophysics. At low baryon chemical potential and high temperature, lattice quantum chromodynamics (QCD) and ultrarelativistic heavy-ion experiments have established that the transition from hadronic matter to the quark-gluon plasma is an analytic crossover (Aoki et al. 2006; Cheng et al. 2006; Aoki et al. 2009; Borsanyi et al. 2014; Bazavov et al. 2014). At low temperature and high baryon density, however, first-principles lattice calculations are obstructed by the sign problem (Alford et al. 1999; Hands 2007). Whether cold dense QCD matter contains a strong first-order phase transition (FOPT), characterized here by a vanishing sound speed over a finite density interval (Glendenning 1992), is therefore still unknown from first principles.

Neutron stars provide the most direct observational access to cold dense matter. Recent multi-messenger measurements have substantially narrowed the uncertainties of equation of state (EOS) of cold dense β -equilibrated matter. In particular, the gravitational wave signal GW170817 from the binary neutron-star merger constrains the tidal deformability of canonical-mass neutron stars (Abbott et al. 2017, 2019), while the Neutron Star Interior Composition Explorer (NICER) provides simultaneous mass–radius measurements for several pulsars through pulse-profile modeling. The NICER measurement of the high-mass pulsar PSR J0740+6620 (Miller et al. 2021; Riley et al. 2021; Salmi et al. 2024a) yields a mass $M \simeq 2.08 M_\odot$ that places a stringent lower bound on the neutron-star maximum mass, while its measured radius constrains the EOS at high density. The lower-mass NICER sources PSR J0030+0451 (Miller et al. 2019; Riley et al. 2019; Vinciguerra et al. 2024), PSR J0437–4715 (Choudhury et al. 2024a; Reardon et al. 2024), and PSR J0614–3329 (Mauviard et al. 2025a) further constrain the neutron-star radii in the canonical-mass regime. Together, current observations

probe the EOS of neutron-star matter over baryon densities of roughly $3\text{--}8n_0$ reached inside stable neutron stars.

Theoretical calculations constrain the EOS in complementary density regimes. At low density, chiral effective field theory (ChEFT) provides controlled calculations up to $\sim 1\text{--}2n_0$, with quantified many-body and truncation uncertainties (Tews et al. 2013; Hebeler et al. 2013; Lynn et al. 2016; Drischler et al. 2019, 2020; Keller et al. 2023). At very high density, perturbative QCD (pQCD) provides a weak-coupling calculation of the EOS once the quark chemical potential is sufficiently large (Freedman & McLerran 1977; Kurkela et al. 2010; Kurkela & Vuorinen 2016; Gorda et al. 2018, 2021, 2023c). Although pQCD thermodynamics becomes quantitatively reliable only at extremely high densities of order $40n_0$, causality and thermodynamic stability allow the high-density constraint to be propagated downward (Komoltsev & Kurkela 2022). Recent work has shown that the pQCD speed of sound remains well converged down to about $25n_0$ (Gorda et al. 2023c), extending the validity range of pQCD toward lower densities. Nevertheless, in the broad density range between the ChEFT and pQCD regimes, it is still unclear whether the EOS varies smoothly (no strong first-order phase transition, NPT) or contains an FOPT.

These observational and theoretical inputs have sparked extensive studies of the FOPT in cold dense QCD matter. Most analyses (Alford et al. 2013; Alvarez-Castillo & Blaschke 2017; Ayriyan et al. 2018; Sieniawska et al. 2019; Montana et al. 2019; Han & Steiner 2019; Christian & Schaffner-Bielich 2020; Pang et al. 2020; Blacker et al. 2020; Annala et al. 2020; Tang et al. 2021; Tan et al. 2022; Gorda et al. 2023a; Brandes et al. 2023; Takatsy et al. 2023; Essick et al. 2023; Kumar et al. 2023; Annala et al. 2023; Christian et al. 2024; Zhou et al. 2024; Saha & Mallick 2024; Ayriyan et al. 2025; Grundler & Li 2025; Verma et al. 2025; Ji et al. 2025; Li et al. 2025; Lindblom et al. 2025; Hammond et al. 2026; Ecker et al. 2026), however, do not directly compare the FOPT and NPT hypotheses through Bayesian model selection. Such a comparison is carried out in only a few studies (Pang et al. 2021; Komoltsev 2024; Huang & Sourav 2025; Tang et al. 2025), but the FOPT onset density they consider is generally restricted to densities reached in neutron-star interiors. It is therefore worthwhile to test the FOPT hypothesis over a broader density range that spans the full ChEFT–pQCD window.

In this work, we perform Bayesian inference using a non-parametric Gaussian-process (GP) EOS for cold β -equilibrated neutron-star matter. The inference combines the tidal deformability of

GW170817, NICER mass–radius measurements of PSR J0740+6620, PSR J0030+0451, PSR J0437–4715, and PSR J0614–3329, ChEFT below $1.5n_0$, and pQCD constraints. The GP EOS is terminated at $n_L = 25n_0$ to span the full ChEFT–pQCD window, with a lower choice $n_L = 12n_0$ examined for comparison. Comparing the NPT hypothesis with the FOPT hypothesis in which $c_s^2 = 0$ over a finite density interval, we find moderate evidence in favor of an FOPT against NPT, with the FOPT onset density most likely located above the central density of the maximum-mass neutron star.

This paper is organized as follows. Section 2 describes the Gaussian-process EOS construction and the Bayesian framework combining GW170817, NICER, ChEFT, and pQCD constraints. Section 3 presents the inferred FOPT properties and their implications for the EOS, stellar observables, and the location of the transition relative to stable neutron-star interiors. Section 4 summarizes the main conclusions.

2. METHODS

2.1. Physics-agnostic EOS

To construct a physics-agnostic and non-parametric EOS of cold β -equilibrated neutron-star matter, we model its squared sound speed $c_s^2(n)$ at baryon number density n with GP regression (Rasmussen & Williams 2006). Causality and thermodynamic stability bound c_s^2 to $[0, 1]$, so we place the GP prior on the auxiliary variable $\phi(n) \equiv -\ln[1/c_s^2(n) - 1]$ rather than on c_s^2 itself,

$$\phi(n) \sim \mathcal{GP}(\bar{\phi}, K(n, n')), \quad \bar{\phi} \equiv -\ln[1/\bar{c}_s^2 - 1], \quad (1)$$

with squared-exponential kernel $K(n, n') = \eta \exp[-(n - n')^2/(2\ell^2)]$. The hyperprior distributions are (Gorda et al. 2023b)

$$\begin{aligned} \ell &\sim \mathcal{N}(1.0n_0, (0.25n_0)^2), \\ \eta &\sim \mathcal{N}(1.25, 0.2^2), \\ \bar{c}_s^2 &\sim \mathcal{N}(0.5, 0.25^2). \end{aligned} \quad (2)$$

The GP variable $\phi(n)$ is predicted over densities from a crust-matching density $n_{cc} = 0.5n_0$ up to a termination density n_L . Since pQCD constrains a nonzero c_s^2 down to $25n_0$ (e.g., Fig. 10 of Komoltsev et al. 2024), we set $n_L = 25n_0$ to span the full ChEFT–pQCD interval. We also examine $n_L = 12n_0$ for comparison.

The GP of Eq. (1) is conditioned on theoretical calculations at a set of training densities $\mathbf{n}_t = \mathcal{T}_{\text{ChEFT}} \cup \mathcal{T}_{\text{pQCD}}$, comprising a low-density ChEFT subset $\mathcal{T}_{\text{ChEFT}}$ and a high-density pQCD subset $\mathcal{T}_{\text{pQCD}}$. The ChEFT subset is a grid aligned with the next-to-next-to-next-to-leading-order (N^3LO) ChEFT calculation of Keller

et al. (2023), spanning $0.58 n_0 \leq n \leq 1.5 n_0$. At each $n_t \in \mathcal{T}_{\text{ChEFT}}$, the mean $c_{s,t}^2$ is the midpoint of the softest and stiffest ChEFT sound speeds, and σ_t is fixed so that the 90% interval of $\mathcal{N}(c_{s,t}^2, \sigma_t^2)$ matches the ChEFT band. The pQCD subset $\mathcal{T}_{\text{pQCD}} = \{25 n_0\}$ anchors the GP to the pQCD prediction at $25 n_0$, where $c_s^2(25 n_0) \sim \mathcal{N}(c_{s,t}^2, \sigma_t^2)$. Following Komoltsev et al. (2024), we take $c_{s,t}^2 = 0.32 c^2$ as the mean and $\sigma_t = 0.05 c^2$ as twice the standard deviation of the pQCD predictions at $25 n_0$ (Komoltsev 2023).

Each $c_s^2(n)$ realization is drawn from the GP conditioned on the training data. The training inputs are mapped into the GP variable through $\phi_t = \phi(c_{s,t}^2)$, while propagating σ_t through ϕ gives the diagonal training covariance $\Sigma_t = \text{diag}\left\{\frac{1}{4} [\phi(c_{s,t}^2 + \sigma_t) - \phi(c_{s,t}^2 - \sigma_t)]^2\right\}$. Conditioning the GP prior on ϕ_t and Σ_t then yields the predicted values $\phi_\star \equiv \phi(\mathbf{n}_\star)$ at prediction densities $\mathbf{n}_\star \in [n_{\text{cc}}, n_L]$, following a multivariate Gaussian,

$$p(\phi_\star | \phi_t, \Sigma_t) = \mathcal{N}(\boldsymbol{\mu}_\star, \boldsymbol{\Sigma}_\star), \quad (3)$$

with mean and covariance

$$\boldsymbol{\mu}_\star = \bar{\phi} + \mathbf{K}(\mathbf{n}_\star, \mathbf{n}_t) \mathbf{C}^{-1} (\phi_t - \bar{\phi}), \quad (4)$$

$$\boldsymbol{\Sigma}_\star = \mathbf{K}(\mathbf{n}_\star, \mathbf{n}_\star) - \mathbf{K}(\mathbf{n}_\star, \mathbf{n}_t) \mathbf{C}^{-1} \mathbf{K}(\mathbf{n}_t, \mathbf{n}_\star), \quad (5)$$

where $\mathbf{C} \equiv \mathbf{K}(\mathbf{n}_t, \mathbf{n}_t) + \Sigma_t$. Sampling ϕ_\star from $p(\phi_\star | \phi_t, \Sigma_t)$ and inverting the map ϕ yields $c_s^2(n)$.

The construction above corresponds to the NPT hypothesis, where the GP yields a smooth $c_s^2(n)$ throughout $[n_{\text{cc}}, n_L]$. For the FOPT, we sample two additional densities independently from a uniform distribution on $[1.5 n_0, n_L]$ and label the smaller and larger as n_S and n_E . The sound speed vanishes between them,

$$c_s^2(n) = 0, \quad n_S \leq n \leq n_E. \quad (6)$$

We then draw two independent GP realizations over $[n_{\text{cc}}, n_L]$ and take the first on $[n_{\text{cc}}, n_S]$ and the second on $[n_E, n_L]$, leaving the sound speed on the two sides of the transition uncorrelated.

Once $c_s^2(n)$ is specified for $n \geq n_{\text{cc}}$ under either hypothesis, the EOS follows from the thermodynamic relations

$$\mu(n) = \mu(n_{\text{cc}}) \exp\left[\int_{n_{\text{cc}}}^n dn' \frac{c_s^2(n')}{n'}\right], \quad (7)$$

$$\varepsilon(n) = \varepsilon(n_{\text{cc}}) + \int_{n_{\text{cc}}}^n dn' \mu(n'), \quad (8)$$

$$p(n) = -\varepsilon(n) + \mu(n) n, \quad (9)$$

where μ , ε , and p denote the baryon chemical potential, energy density, and pressure, respectively. For $n \leq n_{\text{cc}}$,

we adopt the crust EOS (Baym et al. 1971; Negele & Vautherin 1973), which fixes the boundary values $\mu(n_{\text{cc}})$ and $\varepsilon(n_{\text{cc}})$ in Eqs. (7) and (8).

We solve the Tolman–Oppenheimer–Volkoff equations (Tolman 1939; Oppenheimer & Volkoff 1939) for each EOS sample to obtain the neutron-star mass–radius relation and the central baryon density n_c of the most massive configuration. Within the FOPT hypothesis, we further distinguish whether the transition occurs inside stable neutron stars. Samples with $n_S < n_c$ are labeled FOPT-in, while samples with $n_S \geq n_c$ are labeled FOPT-out. The dimensionless tidal deformability Λ is obtained from the $\ell = 2$ tidal Love number k_2 (Hinderer 2008). Under the FOPT hypothesis, the energy-density discontinuity $\Delta\varepsilon$ at the transition radius r_d shifts the metric perturbation variable $y \equiv rH'/H$ by $\Delta y = -4\pi r_d^3 \Delta\varepsilon / [m(r_d) + 4\pi r_d^3 p(r_d)]$ (Postnikov et al. 2010), which we incorporate when integrating k_2 across the transition.

2.2. Bayesian inference

We combine the theoretical and observational information in a hierarchical Bayesian framework. For data \vec{d} and hypothesis \mathcal{H} , the posterior for the EOS parameters θ is (Thrane & Talbot 2019; Hernandez Vivanco et al. 2020)

$$p(\theta | \vec{d}, \mathcal{H}) = \frac{\prod_i \mathcal{L}(d_i | \theta, \mathcal{H}) \pi(\theta | \mathcal{H})}{\mathcal{Z}_{\mathcal{H}}(\vec{d})}, \quad (10)$$

where i runs over independent constraints and $\pi(\theta | \mathcal{H})$ denotes the prior under hypothesis \mathcal{H} . The evidence is

$$\mathcal{Z}_{\mathcal{H}}(\vec{d}) \equiv \int \prod_i \mathcal{L}(d_i | \theta, \mathcal{H}) \pi(\theta | \mathcal{H}) d\theta, \quad (11)$$

and it quantifies the support that the data give to the hypothesis. We compare two hypotheses through the Bayes factor (Jeffreys 1939; Lee & Wagenmakers 2014)

$$\mathcal{B}_2^1 = \mathcal{Z}_1(\vec{d}) / \mathcal{Z}_2(\vec{d}). \quad (12)$$

On the Jeffreys scale (Jeffreys 1939; Trotta 2008; Lee & Wagenmakers 2014), \mathcal{B}_2^1 in the ranges $[1, 3]$, $[3, 10]$, $[10, 30]$, $[30, 100]$, and $[100, \infty)$ corresponds to anecdotal, moderate, strong, very strong, and extreme evidence, respectively, in favor of hypothesis 1.

For each NICER mass–radius measurement, the likelihood is obtained by marginalizing a kernel density estimate of the published mass–radius posterior over the neutron-star mass along the EOS-predicted curve $R(m, \theta)$. The analysis includes PSR J0740+6620 (Salmi et al. 2024a,b),

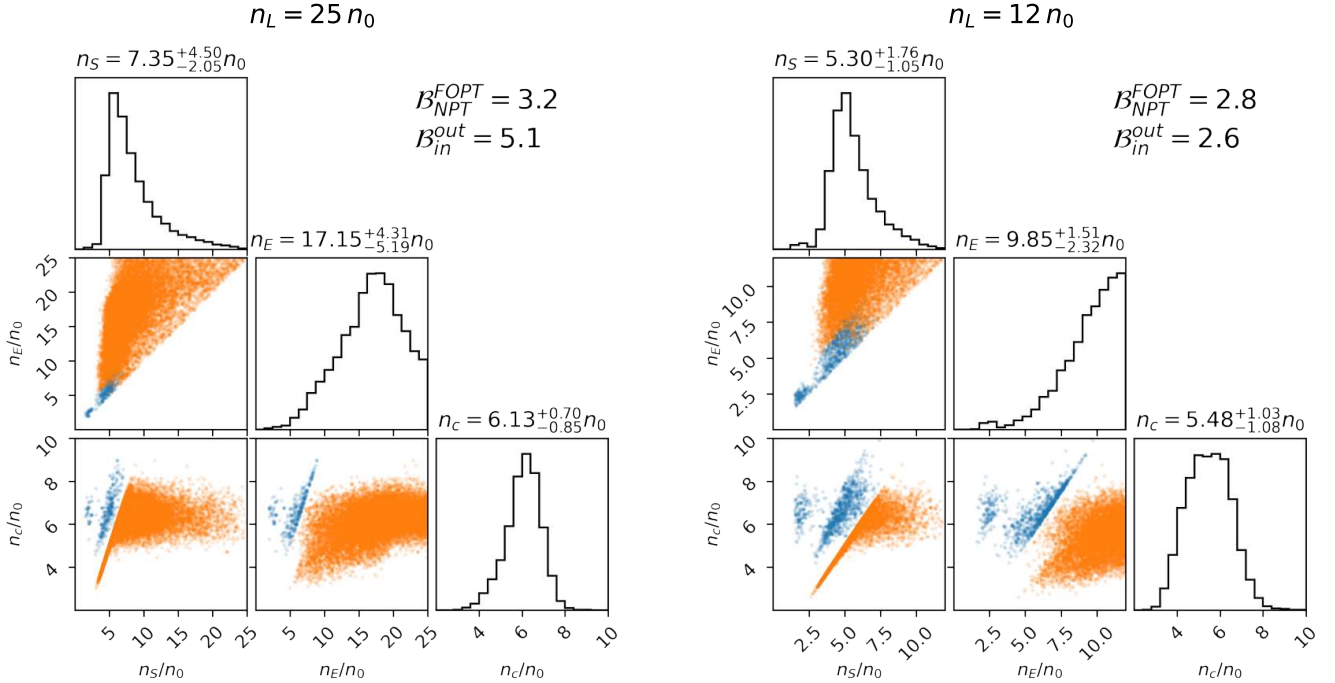


Figure 1. Corner plots of the posterior distributions of the FOPT onset density n_S , end density n_E , and central density n_c of the most massive neutron star for the two choices of n_L : $n_L = 25 n_0$ (left panel) and $n_L = 12 n_0$ (right panel). In each panel, the diagonal subpanels show the one-dimensional marginalized posteriors, with the median and 68% credible interval reported in each panel title; the Bayes factors B_{NPT}^{FOPT} and B_{in}^{out} are also annotated. The off-diagonal panels display equally-weighted posterior samples, with blue ($n_S < n_c$) and orange ($n_S \geq n_c$) marking FOPT onsets below and above n_c , respectively.

PSR J0030+0451 (ST+PDT hot-spot model) (Vinciguerra et al. 2023, 2024), PSR J0437–4715 (Choudhury et al. 2024a,b), and PSR J0614–3329 (Mauviard et al. 2025a,b). For the tidal deformability from GW170817 (Abbott et al. 2017, 2019), we adopt the nuisance-marginalized likelihood of Hernandez Vivanco et al. (2020) under the low-spin prior and marginalize over the component masses along the EOS-predicted curve $\Lambda(m, \theta)$.

The above astrophysical likelihoods constrain the EOS only within stable neutron stars ($n \lesssim 5\text{--}8 n_0$). To extend the constraint to higher densities, we adopt the marginalized pQCD likelihood of Komoltsev et al. (2024, 2025). The likelihood is built from an auxiliary Gaussian process GP_{aux} , anchored to the pQCD thermodynamic quantities at $n_{\text{pQCD}} \simeq 40 n_0$ (Gorda et al. 2021) and conditioned on the pQCD-predicted $c_s^2(n)$ over $25 n_0 \leq n \leq 40 n_0$, where perturbative corrections remain small (Gorda et al. 2023c). For any $n_m \leq 25 n_0$, marginalizing GP_{aux} over $[n_m, n_{\text{pQCD}}]$ yields a joint distribution of (p, ε) at n_m , which defines the marginalized pQCD likelihood at n_m . We evaluate this likelihood directly at the EOS termination density n_L , i.e., $n_m = n_L$, thereby constraining the entire EOS below n_L . Two caveats are in order. First, the pQCD likelihood con-

strains (p, ε) at n_L , reflecting the integral of c_s^2 up to n_L rather than $c_s^2(n_L)$ itself. Second, GP_{aux} is smooth by construction and therefore does not model an FOPT between n_L and n_{pQCD} .

We evaluate posteriors and evidences by importance sampling. For each hypothesis \mathcal{H} and each value of n_L , we draw $N = 8 \times 10^6$ samples $\{\theta_k\}$ from the prior and assign each a weight $w_k = \prod_i \mathcal{L}(d_i | \theta_k, \mathcal{H})$. The evidence then follows as $\mathcal{Z}_{\mathcal{H}}(\vec{d}) \simeq N^{-1} \sum_k w_k$, and the effective sample size (Kong et al. 1994), $N_{\text{eff}} = (\sum_k w_k)^2 / \sum_k w_k^2$, exceeds 1×10^4 in all four runs (the FOPT and NPT hypotheses at $n_L = 25 n_0$ and $12 n_0$), ensuring convergence of the posterior estimates. Equally-weighted posterior samples are then obtained by resampling with replacement according to w_k , from which posterior distributions are computed.

3. RESULTS AND DISCUSSION

For $n_L = 25 n_0$, we find $B_{NPT}^{FOPT} = 3.2$, corresponding to moderate evidence on the Jeffreys scale for the FOPT hypothesis relative to the NPT hypothesis. The posterior distributions of the FOPT onset density n_S , end density n_E , and the central density n_c of the maximum-mass neutron star are shown in Fig. 1, where blue and orange samples correspond to the FOPT-in ($n_S < n_c$) and FOPT-out ($n_S \geq n_c$), respectively. Within the

FOPT hypothesis, the data further favor FOPT-out over FOPT-in, with $\mathcal{B}_{\text{in}}^{\text{out}} = 5.1$. Together, for $n_L = 25 n_0$, the data support an FOPT whose onset most likely lies above the central density of the maximum-mass neutron star. Placing the FOPT onset above n_c agrees with earlier physics-agnostic inferences that incorporate heavy pulsars and find no sharp sound-speed drop within massive neutron-star cores (Somasundaram et al. 2023; Brandes et al. 2023). This agreement reflects a common physical tension: supporting massive neutron stars demands a stiff EOS in their interiors, while a strong FOPT would soften the EOS.

For comparison, we also perform the inference with a more restricted extrapolation boundary $n_L = 12 n_0$. In this case, the support for the FOPT hypothesis drops to $\mathcal{B}_{\text{NPT}}^{\text{FOPT}} = 2.8$, only anecdotal on the Jeffreys scale. The preference for FOPT-out also weakens, from $\mathcal{B}_{\text{in}}^{\text{out}} = 5.1$ at $n_L = 25 n_0$ to 2.6 at $n_L = 12 n_0$. Because the marginalized pQCD likelihood is built from a smooth auxiliary GP above n_L , lowering n_L from $25 n_0$ to $12 n_0$ excludes any FOPT in the density range $12 n_0 < n < 25 n_0$ and thereby reduces both Bayes factors. Even within this restricted window, nevertheless, the data still mildly favor an FOPT against NPT with the FOPT onset density lying above n_c .

The FOPT hypothesis shifts the maximum mass of a nonrotating neutron star M_{TOV} modestly upward relative to the NPT. This shift is visible at the upper edge of the mass–radius contour in Fig. 2(a), where $M_{\text{TOV}}^{\text{NPT}} = 2.07_{-0.08}^{+0.10} M_{\odot}$ (68% credible interval, here and throughout unless stated otherwise) rises to $M_{\text{TOV}}^{\text{FOPT}} = 2.15_{-0.11}^{+0.13} M_{\odot}$ for $n_L = 25 n_0$. It should be noted that the marginalized pQCD likelihood at n_L disfavors stiff EOSs and is therefore in tension with the stiffness required to support a $\sim 2 M_{\odot}$ neutron star. An FOPT resolves this tension. The $c_s^2 = 0$ plateau softens the EOS and relaxes the pQCD penalty, while the inferred onset lies predominantly above n_c , leaving the stellar interior stiff enough for M_{TOV} to readily satisfy the PSR J0740+6620 mass constraint.

Although the FOPT hypothesis raises M_{TOV} , the canonical-mass observables remain essentially unchanged. For $n_L = 25 n_0$ we obtain $R_{1.4}^{\text{FOPT}} = 11.76_{-0.38}^{+0.38}$ km versus $R_{1.4}^{\text{NPT}} = 11.79_{-0.41}^{+0.37}$ km, and $\Lambda_{1.4}^{\text{FOPT}} = 309_{-70}^{+88}$ versus $\Lambda_{1.4}^{\text{NPT}} = 317_{-75}^{+86}$ [panel (c) of Fig. 2]—the two hypotheses are statistically indistinguishable at the 68% level. Earlier analyses that assume an FOPT at $2\text{--}3 n_0$ soften the EOS at canonical-mass densities and drive $R_{1.4}$ down to ~ 10 km (Steiner et al. 2013, 2018). In our analysis, by contrast, n_S is inferred rather than imposed, and the posterior favors an onset above the central density of the most massive neutron

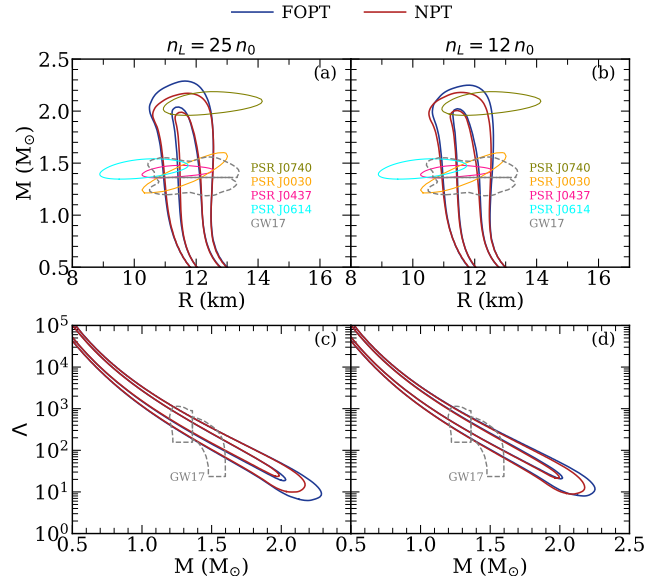


Figure 2. Joint posterior distributions of mass–radius (top) and tidal deformability–mass (bottom) for neutron stars under the FOPT (blue) and NPT (red) hypotheses, shown as 68% and 95% credible regions. The left (right) column is for $n_L = 25 n_0$ ($12 n_0$). Astrophysical constraints—NICER joint posteriors for PSR J0740+6620 (Salimi et al. 2024a), PSR J0030+0451 (Vinciguerra et al. 2024), PSR J0437–4715 (Choudhury et al. 2024a), and PSR J0614–3329 (Mauviard et al. 2025a), together with the GW170817 posterior (Abbott et al. 2018)—are overlaid for reference.

star, leaving the canonical-mass interior essentially unaffected.

Figure 2(b) and (d) show the mass–radius and tidal-deformability–mass joint posteriors for $n_L = 12 n_0$, which reproduce the qualitative conclusions established at $n_L = 25 n_0$. The canonical-mass observables remain statistically indistinguishable between the two hypotheses at the 68% level, with $R_{1.4}^{\text{FOPT}} = 11.79_{-0.39}^{+0.39}$ km versus $R_{1.4}^{\text{NPT}} = 11.75_{-0.39}^{+0.39}$ km and $\Lambda_{1.4}^{\text{FOPT}} = 314_{-71}^{+92}$ versus $\Lambda_{1.4}^{\text{NPT}} = 308_{-70}^{+89}$. The modest FOPT-driven upward shift in the maximum mass also persists for $n_L = 12 n_0$, from $M_{\text{TOV}}^{\text{NPT}} = 2.08_{-0.08}^{+0.10} M_{\odot}$ to $M_{\text{TOV}}^{\text{FOPT}} = 2.14_{-0.10}^{+0.12} M_{\odot}$.

Because the inferred FOPT onset lies predominantly above n_c , the transition leaves no direct imprint on cold, stable neutron stars. The FOPT and NPT posteriors for $R_{1.4}$ and $\Lambda_{1.4}$ agree at the 68% level for either choice of n_L , and their M_{TOV} values differ by only $\Delta M_{\text{TOV}} \simeq 0.06\text{--}0.08 M_{\odot}$. Another classical signature of an FOPT—a disconnected “twin-star” branch supporting two stable stellar configurations of equal mass but different radii—is likewise strongly disfavored by our analyses. We find that the posterior probability of a twin-star solution under the FOPT hypothesis

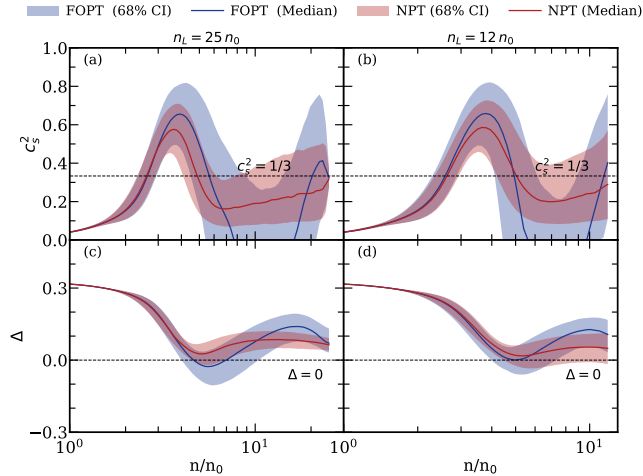


Figure 3. Squared sound speed c_s^2 (top) and trace anomaly $\Delta = 1/3 - p/\epsilon$ (bottom) as functions of baryon density, with $n_L = 25 n_0$ in the left column and $n_L = 12 n_0$ in the right column. Filled bands give the 68% credible intervals and solid lines mark the median values, with FOPT shown in blue and NPT in red. Black dashed lines indicate the conformal references $c_s^2 = c^2/3$ and $\Delta = 0$.

is $\leq 0.1\%$ for both $n_L = 25 n_0$ and $12 n_0$, in agreement with the model-agnostic exclusion of twin stars reported in Blomqvist et al. (2025). Direct tests of an FOPT should therefore target systems that briefly access densities beyond the central density of the most massive stable neutron star. Binary neutron-star post-merger gravitational-wave emission, targeted by next-generation observatories (Maggiore et al. 2020; Ackley et al. 2020; Evans et al. 2021), offers a natural candidate: the transient remnant briefly attains densities exceeding n_c , and an FOPT triggered above n_c would imprint itself on the gravitational-wave signal through a shift in the dominant post-merger frequency and a reduced remnant lifetime (Bauswein et al. 2019; Most et al. 2019; Weih et al. 2020; Fujimoto et al. 2023).

Figure 3(a) shows the posterior $c_s^2(n)$ for $n_L = 25 n_0$ under the NPT and FOPT hypotheses. At low densities, c_s^2 rises under both hypotheses with essentially overlapping posteriors, consistent with the indistinguishable $R_{1.4}$ and $\Lambda_{1.4}$. At higher densities, c_s^2 develops a peak near $\sim 4 n_0$ and decreases before reaching $n_c \simeq 6 n_0$ in either case. Under the FOPT, both the peak c_s^2 and its value at n_c exceed those under the NPT, reflecting a stiffer neutron-star interior that the pQCD constraint does not overly soften. Beyond the peak, the two posteriors approach the pQCD-predicted value ($\simeq 0.32 c^2$) along distinct routes: the NPT descends to a minimum of $\sim 0.2 c^2$ near n_c and then rises smoothly toward the pQCD-predicted value from below, whereas the FOPT drops to zero across the plateau, rebounds to a smaller

Table 1. Posterior medians and 68% credible intervals for the two choices of n_L under both the FOPT and NPT hypotheses. The maximum nonrotating mass M_{TOV} , the radius $R_{1.4}$, the tidal deformability $\Lambda_{1.4}$, and the central density n_c of the most massive neutron star are reported under both hypotheses. The FOPT onset density n_S , FOPT end density n_E , and the two Bayes factors $\mathcal{B}_{\text{NPT}}^{\text{FOPT}}$ (FOPT versus NPT) and $\mathcal{B}_{\text{in}}^{\text{out}}$ (FOPT-out versus FOPT-in) are reported only under the FOPT hypothesis.

Quantity	$n_L = 25 n_0$		$n_L = 12 n_0$	
	NPT	FOPT	NPT	FOPT
M_{TOV}/M_\odot	$2.07^{+0.10}_{-0.08}$	$2.15^{+0.13}_{-0.11}$	$2.08^{+0.10}_{-0.08}$	$2.14^{+0.12}_{-0.10}$
$R_{1.4}/\text{km}$	$11.79^{+0.37}_{-0.41}$	$11.76^{+0.38}_{-0.38}$	$11.75^{+0.39}_{-0.39}$	$11.79^{+0.39}_{-0.39}$
$\Lambda_{1.4}$	317^{+86}_{-75}	309^{+88}_{-70}	308^{+89}_{-70}	314^{+92}_{-71}
n_c/n_0	$6.24^{+0.62}_{-0.57}$	$6.13^{+0.70}_{-0.85}$	$6.32^{+0.61}_{-0.57}$	$5.48^{+1.03}_{-1.08}$
n_S/n_0	—	$7.35^{+4.50}_{-2.05}$	—	$5.30^{+1.76}_{-1.05}$
n_E/n_0	—	$17.15^{+4.31}_{-5.19}$	—	$9.85^{+1.51}_{-2.32}$
$\mathcal{B}_{\text{NPT}}^{\text{FOPT}}$	—	3.2	—	2.8
$\mathcal{B}_{\text{in}}^{\text{out}}$	—	5.1	—	2.6

post-plateau peak, and approaches the pQCD-predicted value from above. The post-plateau c_s^2 peak under the FOPT indicates that the matter beyond the FOPT remains markedly non-conformal over an extended window before joining the perturbative regime.

A complementary diagnostic of conformality is the trace anomaly $\Delta \equiv 1/3 - p/\epsilon$ (Fujimoto et al. 2022), shown in Fig. 3(c) for $n_L = 25 n_0$. Under the FOPT hypothesis, Δ first decreases to a dip, then rises monotonically to a pronounced maximum before approaching the perturbative regime from above, whereas the NPT posterior follows the same pattern with a markedly weaker rebound. Moreover, Δ does not flatten toward zero below $n_c \simeq 6 n_0$ under either hypothesis, indicating that the matter inside neutron stars remains non-conformal and strongly coupled.

Figure 3(b) and (d) display $c_s^2(n)$ and $\Delta(n)$ for $n_L = 12 n_0$. Below $\sim 5 n_0$, both panels closely follow their $n_L = 25 n_0$ counterparts: c_s^2 rises to a peak near $\sim 4 n_0$ that is more pronounced under the FOPT, while Δ descends toward a dip. At higher densities, the lower extrapolation boundary leaves a clear imprint on the FOPT plateau. The plateau is markedly narrower than for $n_L = 25 n_0$: the median width is $n_E - n_S \simeq (9.9 - 5.3) n_0 = 4.6 n_0$ at $n_L = 12 n_0$ versus $(17.2 - 7.4) n_0 = 9.8 n_0$ at $n_L = 25 n_0$, so a lower n_L compresses the density window available to the transition. For both choices of n_L , Table 1 summarizes the

posterior medians and credible intervals of the stellar observables and characteristic densities, together with the Bayes factors.

Finally, we would like to mention that the $c_s^2 = 0$ plateau under the FOPT actually follows from the Maxwell construction, in which each pure phase is separately charge-neutral and β -equilibrated. The NPT hypothesis instead yields a smooth $c_s^2(n)$ that can in principle describe a continuous crossover from hadronic to quark matter. In addition, an alternative treatment of the phase coexistence is the Gibbs construction, in which charge neutrality is imposed globally and the two phases coexist throughout a mixed phase (Glendenning 1992). The resulting $c_s^2(n)$ stays nonzero across the mixed phase and develops kinks at the lower and upper transition densities. Extending our framework to the Gibbs construction is a natural next step toward a more complete characterization of the dense-matter phase transition.

4. SUMMARY

We have performed Bayesian inference with a non-parametric Gaussian-process EOS for β -equilibrated neutron-star matter, using the GW170817 tidal deformability, the NICER mass-radius measurements of PSR J0740+6620, PSR J0030+0451, PSR J0437-4715, and PSR J0614-3329, ChEFT below $1.5n_0$, and the pQCD sound speed over $25n_0 \leq n \leq 40n_0$ together with the pQCD thermodynamic quantities at $n_{\text{pQCD}} \simeq 40n_0$. Within this framework, we have tested the strong first-order phase transition (FOPT) hypothesis directly against the no strong first-order phase transition (NPT) hypothesis and further tested whether the FOPT onset density lies above (FOPT-out) or below (FOPT-in) the central density of the most massive neutron star.

With the Gaussian-process EOS terminated at $n_L = 25n_0$, the data moderately favor the FOPT hypothesis

over NPT and FOPT-out over FOPT-in, with $\mathcal{B}_{\text{NPT}}^{\text{FOPT}} = 3.2$ and $\mathcal{B}_{\text{in}}^{\text{out}} = 5.1$. Lowering the termination density to $n_L = 12n_0$ gives a consistent but weaker preference, with $\mathcal{B}_{\text{NPT}}^{\text{FOPT}} = 2.8$ and $\mathcal{B}_{\text{in}}^{\text{out}} = 2.6$. These Bayes factors collectively favor the FOPT hypothesis, with the onset most likely *beyond* the densities reached inside stable neutron stars. Because the inferred FOPT onset predominantly lies above the central density n_c , the canonical-mass observables $R_{1.4}$ and $\Lambda_{1.4}$ are statistically indistinguishable between the two hypotheses.

Generally, the pQCD constraint disfavors stiff EOSs, in tension with the stiffness required to support a $\sim 2M_\odot$ neutron star. An FOPT predominantly lying above n_c prevents the neutron-star interior from softening excessively under the pQCD constraint and shifts M_{TOV} modestly upward, while allowing the EOS to soften toward the pQCD regime at higher densities, and thus appears to provide a natural resolution of this tension. Future gravitational-wave observations of binary neutron-star mergers, in particular the post-merger signal accessible to next-generation detectors (Maggiore et al. 2020; Ackley et al. 2020; Evans et al. 2021), may further test our present conclusion.

ACKNOWLEDGEMENTS

We thank Sophia Han and Zhen Zhang for helpful discussions. This work was supported by the National Natural Science Foundation of China under Grant No. 12235010, the National SKA Program of China No. 2020SKA0120300, and the Science and Technology Commission of Shanghai. The computations in this paper were run on the Siyuan-1 cluster supported by the Center for High Performance Computing at Shanghai Jiao Tong University.

REFERENCES

- Abbott, B. P., et al. 2017, Phys. Rev. Lett., 119, 161101, doi: [10.1103/PhysRevLett.119.161101](https://doi.org/10.1103/PhysRevLett.119.161101)
- . 2018, Phys. Rev. Lett., 121, 161101, doi: [10.1103/PhysRevLett.121.161101](https://doi.org/10.1103/PhysRevLett.121.161101)
- . 2019, Phys. Rev. X, 9, 011001, doi: [10.1103/PhysRevX.9.011001](https://doi.org/10.1103/PhysRevX.9.011001)
- Ackley, K., et al. 2020, Publ. Astron. Soc. Austral., 37, e047, doi: [10.1017/pasa.2020.39](https://doi.org/10.1017/pasa.2020.39)
- Alford, M. G., Han, S., & Prakash, M. 2013, Phys. Rev. D, 88, 083013, doi: [10.1103/PhysRevD.88.083013](https://doi.org/10.1103/PhysRevD.88.083013)
- Alford, M. G., Kapustin, A., & Wilczek, F. 1999, Phys. Rev. D, 59, 054502, doi: [10.1103/PhysRevD.59.054502](https://doi.org/10.1103/PhysRevD.59.054502)
- Alvarez-Castillo, D. E., & Blaschke, D. B. 2017, Phys. Rev. C, 96, 045809, doi: [10.1103/PhysRevC.96.045809](https://doi.org/10.1103/PhysRevC.96.045809)
- Annala, E., Gorda, T., Hirvonen, J., et al. 2023, Nature Commun., 14, 8451, doi: [10.1038/s41467-023-44051-y](https://doi.org/10.1038/s41467-023-44051-y)
- Annala, E., Gorda, T., Kurkela, A., Nättilä, J., & Vuorinen, A. 2020, Nature Phys., 16, 907, doi: [10.1038/s41567-020-0914-9](https://doi.org/10.1038/s41567-020-0914-9)
- Aoki, Y., Borsanyi, S., Durr, S., et al. 2009, JHEP, 06, 088, doi: [10.1088/1126-6708/2009/06/088](https://doi.org/10.1088/1126-6708/2009/06/088)
- Aoki, Y., Endrodi, G., Fodor, Z., Katz, S. D., & Szabo, K. K. 2006, Nature, 443, 675, doi: [10.1038/nature05120](https://doi.org/10.1038/nature05120)
- Ayriyan, A., Bastian, N. U., Blaschke, D., et al. 2018, Phys. Rev. C, 97, 045802, doi: [10.1103/PhysRevC.97.045802](https://doi.org/10.1103/PhysRevC.97.045802)

- Ayriyan, A., Ivanytskyi, O., & Blaschke, D. 2025, <https://arxiv.org/abs/2509.02554>
- Bauswein, A., Bastian, N.-U. F., Blaschke, D. B., et al. 2019, *Phys. Rev. Lett.*, 122, 061102, doi: [10.1103/PhysRevLett.122.061102](https://doi.org/10.1103/PhysRevLett.122.061102)
- Baym, G., Pethick, C., & Sutherland, P. 1971, *Astrophys. J.*, 170, 299, doi: [10.1086/151216](https://doi.org/10.1086/151216)
- Bazavov, A., et al. 2014, *Phys. Rev. D*, 90, 094503, doi: [10.1103/PhysRevD.90.094503](https://doi.org/10.1103/PhysRevD.90.094503)
- Blacker, S., Bastian, N.-U. F., Bauswein, A., et al. 2020, *Phys. Rev. D*, 102, 123023, doi: [10.1103/PhysRevD.102.123023](https://doi.org/10.1103/PhysRevD.102.123023)
- Blomqvist, S., Ecker, C., Gorda, T., & Vuorinen, A. 2025, <https://arxiv.org/abs/2512.19477>
- Borsanyi, S., Fodor, Z., Hoelbling, C., et al. 2014, *Phys. Lett. B*, 730, 99, doi: [10.1016/j.physletb.2014.01.007](https://doi.org/10.1016/j.physletb.2014.01.007)
- Brandes, L., Weise, W., & Kaiser, N. 2023, *Phys. Rev. D*, 108, 094014, doi: [10.1103/PhysRevD.108.094014](https://doi.org/10.1103/PhysRevD.108.094014)
- Cheng, M., et al. 2006, *Phys. Rev. D*, 74, 054507, doi: [10.1103/PhysRevD.74.054507](https://doi.org/10.1103/PhysRevD.74.054507)
- Choudhury, D., et al. 2024a, *Astrophys. J. Lett.*, 971, L20, doi: [10.3847/2041-8213/ad5a6f](https://doi.org/10.3847/2041-8213/ad5a6f)
- . 2024b, Reproduction package for: “A NICER View of the Nearest and Brightest Millisecond Pulsar: PSR J0437–4715”, Zenodo, doi: [10.5281/zenodo.13766753](https://doi.org/10.5281/zenodo.13766753)
- Christian, J.-E., & Schaffner-Bielich, J. 2020, *Astrophys. J. Lett.*, 894, L8, doi: [10.3847/2041-8213/ab8af4](https://doi.org/10.3847/2041-8213/ab8af4)
- Christian, J.-E., Schaffner-Bielich, J., & Rosswog, S. 2024, *Phys. Rev. D*, 109, 063035, doi: [10.1103/PhysRevD.109.063035](https://doi.org/10.1103/PhysRevD.109.063035)
- Drischler, C., Furnstahl, R. J., Melendez, J. A., & Phillips, D. R. 2020, *Phys. Rev. Lett.*, 125, 202702, doi: [10.1103/PhysRevLett.125.202702](https://doi.org/10.1103/PhysRevLett.125.202702)
- Drischler, C., Hebeler, K., & Schwenk, A. 2019, *Phys. Rev. Lett.*, 122, 042501, doi: [10.1103/PhysRevLett.122.042501](https://doi.org/10.1103/PhysRevLett.122.042501)
- Ecker, C., Jokela, N., & Järvinen, M. 2026, *Phys. Rev. D*, 113, L041302, doi: [10.1103/x17s-sc9t](https://doi.org/10.1103/x17s-sc9t)
- Essick, R., Legred, I., Chatziioannou, K., Han, S., & Landry, P. 2023, *Phys. Rev. D*, 108, 043013, doi: [10.1103/PhysRevD.108.043013](https://doi.org/10.1103/PhysRevD.108.043013)
- Evans, M., et al. 2021, A Horizon Study for Cosmic Explorer: Science, Observatories, and Community. <https://arxiv.org/abs/2109.09882>
- Freedman, B. A., & McLerran, L. D. 1977, *Phys. Rev. D*, 16, 1169, doi: [10.1103/PhysRevD.16.1169](https://doi.org/10.1103/PhysRevD.16.1169)
- Fujimoto, Y., Fukushima, K., Hotokezaka, K., & Kyutoku, K. 2023, *Phys. Rev. Lett.*, 130, 091404, doi: [10.1103/PhysRevLett.130.091404](https://doi.org/10.1103/PhysRevLett.130.091404)
- Fujimoto, Y., Fukushima, K., McLerran, L. D., & Praszalowicz, M. 2022, *Phys. Rev. Lett.*, 129, 252702, doi: [10.1103/PhysRevLett.129.252702](https://doi.org/10.1103/PhysRevLett.129.252702)
- Glendenning, N. K. 1992, *Phys. Rev. D*, 46, 1274, doi: [10.1103/PhysRevD.46.1274](https://doi.org/10.1103/PhysRevD.46.1274)
- Gorda, T., Hebeler, K., Kurkela, A., Schwenk, A., & Vuorinen, A. 2023a, *Astrophys. J.*, 955, 100, doi: [10.3847/1538-4357/aceefb](https://doi.org/10.3847/1538-4357/aceefb)
- Gorda, T., Komoltsev, O., & Kurkela, A. 2023b, *Astrophys. J.*, 950, 107, doi: [10.3847/1538-4357/acce3a](https://doi.org/10.3847/1538-4357/acce3a)
- Gorda, T., Komoltsev, O., Kurkela, A., & Mazeliauskas, A. 2023c, *JHEP*, 06, 002, doi: [10.1007/JHEP06\(2023\)002](https://doi.org/10.1007/JHEP06(2023)002)
- Gorda, T., Kurkela, A., Paatelainen, R., Säppi, S., & Vuorinen, A. 2021, *Phys. Rev. Lett.*, 127, 162003, doi: [10.1103/PhysRevLett.127.162003](https://doi.org/10.1103/PhysRevLett.127.162003)
- Gorda, T., Kurkela, A., Romatschke, P., Säppi, S., & Vuorinen, A. 2018, *Phys. Rev. Lett.*, 121, 202701, doi: [10.1103/PhysRevLett.121.202701](https://doi.org/10.1103/PhysRevLett.121.202701)
- Grundler, X., & Li, B.-A. 2025, *Phys. Rev. D*, 112, 103012, doi: [10.1103/hsd4-j54y](https://doi.org/10.1103/hsd4-j54y)
- Hammond, P., et al. 2026, *Phys. Rev. D*, 113, 044057, doi: [10.1103/71t3-3t28](https://doi.org/10.1103/71t3-3t28)
- Han, S., & Steiner, A. W. 2019, *Phys. Rev. D*, 99, 083014, doi: [10.1103/PhysRevD.99.083014](https://doi.org/10.1103/PhysRevD.99.083014)
- Hands, S. 2007, *Prog. Theor. Phys. Suppl.*, 168, 253, doi: [10.1143/PTPS.168.253](https://doi.org/10.1143/PTPS.168.253)
- Hebeler, K., Lattimer, J. M., Pethick, C. J., & Schwenk, A. 2013, *Astrophys. J.*, 773, 11, doi: [10.1088/0004-637X/773/1/11](https://doi.org/10.1088/0004-637X/773/1/11)
- Hernandez Vivanco, F., Smith, R., Thrane, E., & Lasky, P. D. 2020, *Mon. Not. Roy. Astron. Soc.*, 499, 5972, doi: [10.1093/mnras/staa3243](https://doi.org/10.1093/mnras/staa3243)
- Hinderer, T. 2008, *Astrophys. J.*, 677, 1216, doi: [10.1086/533487](https://doi.org/10.1086/533487)
- Huang, C., & Sourav, S. 2025, *Astrophys. J.*, 983, 17, doi: [10.3847/1538-4357/adbb67](https://doi.org/10.3847/1538-4357/adbb67)
- Jeffreys, H. 1939, *The Theory of Probability*, Oxford Classic Texts in the Physical Sciences
- Ji, Z., Chen, J., & Wu, G. 2025, <https://arxiv.org/abs/2502.05519>
- Keller, J., Hebeler, K., & Schwenk, A. 2023, *Phys. Rev. Lett.*, 130, 072701, doi: [10.1103/PhysRevLett.130.072701](https://doi.org/10.1103/PhysRevLett.130.072701)
- Komoltsev, O. 2023, QCD-likelihood-function, <https://github.com/OKomoltsev/QCD-likelihood-function>
- . 2024, *Phys. Rev. D*, 110, L071502, doi: [10.1103/PhysRevD.110.L071502](https://doi.org/10.1103/PhysRevD.110.L071502)
- Komoltsev, O., Gorda, T., & Kurkela, A. 2025, Marginalized QCD likelihood function, v3, Zenodo, doi: [10.5281/zenodo.15407795](https://doi.org/10.5281/zenodo.15407795)

- Komoltsev, O., & Kurkela, A. 2022, *Phys. Rev. Lett.*, 128, 202701, doi: [10.1103/PhysRevLett.128.202701](https://doi.org/10.1103/PhysRevLett.128.202701)
- Komoltsev, O., Somasundaram, R., Gorda, T., et al. 2024, *Phys. Rev. D*, 109, 094030, doi: [10.1103/PhysRevD.109.094030](https://doi.org/10.1103/PhysRevD.109.094030)
- Kong, A., Liu, J. S., & Wong, W. H. 1994, *Journal of the American Statistical Association*, 89, 278, doi: [10.1080/01621459.1994.10476469](https://doi.org/10.1080/01621459.1994.10476469)
- Kumar, A., Thapa, V. B., & Sinha, M. 2023, *Phys. Rev. D*, 107, 063024, doi: [10.1103/PhysRevD.107.063024](https://doi.org/10.1103/PhysRevD.107.063024)
- Kurkela, A., Romatschke, P., & Vuorinen, A. 2010, *Phys. Rev. D*, 81, 105021, doi: [10.1103/PhysRevD.81.105021](https://doi.org/10.1103/PhysRevD.81.105021)
- Kurkela, A., & Vuorinen, A. 2016, *Phys. Rev. Lett.*, 117, 042501, doi: [10.1103/PhysRevLett.117.042501](https://doi.org/10.1103/PhysRevLett.117.042501)
- Lee, M. D., & Wagenmakers, E.-J. 2014, *Bayesian Cognitive Modeling: A Practical Course* (Cambridge University Press)
- Li, R., Han, S., Lin, Z., et al. 2025, *Phys. Rev. D*, 111, 074026, doi: [10.1103/PhysRevD.111.074026](https://doi.org/10.1103/PhysRevD.111.074026)
- Lindblom, L., Lewis, S. M., & Weber, F. 2025, *Phys. Rev. D*, 111, 123035, doi: [10.1103/jl1z7-jfc6](https://doi.org/10.1103/jl1z7-jfc6)
- Lynn, J. E., Tews, I., Carlson, J., et al. 2016, *Phys. Rev. Lett.*, 116, 062501, doi: [10.1103/PhysRevLett.116.062501](https://doi.org/10.1103/PhysRevLett.116.062501)
- Maggiore, M., et al. 2020, *JCAP*, 03, 050, doi: [10.1088/1475-7516/2020/03/050](https://doi.org/10.1088/1475-7516/2020/03/050)
- Mauviard, L., et al. 2025a, *Astrophys. J.*, 995, 60, doi: [10.3847/1538-4357/ae145d](https://doi.org/10.3847/1538-4357/ae145d)
- . 2025b, Data and Reproduction package for: “A NICER view of the 1.4 solar-mass edge-on pulsar PSR J0614–3329”, Zenodo, doi: [10.5281/zenodo.17380576](https://doi.org/10.5281/zenodo.17380576)
- Miller, M. C., et al. 2019, *Astrophys. J. Lett.*, 887, L24, doi: [10.3847/2041-8213/ab50c5](https://doi.org/10.3847/2041-8213/ab50c5)
- . 2021, *Astrophys. J. Lett.*, 918, L28, doi: [10.3847/2041-8213/ac089b](https://doi.org/10.3847/2041-8213/ac089b)
- Montana, G., Tolos, L., Hanauske, M., & Rezzolla, L. 2019, *Phys. Rev. D*, 99, 103009, doi: [10.1103/PhysRevD.99.103009](https://doi.org/10.1103/PhysRevD.99.103009)
- Most, E. R., Papenfort, L. J., Dexheimer, V., et al. 2019, *Phys. Rev. Lett.*, 122, 061101, doi: [10.1103/PhysRevLett.122.061101](https://doi.org/10.1103/PhysRevLett.122.061101)
- Negele, J. W., & Vautherin, D. 1973, *Nucl. Phys. A*, 207, 298, doi: [10.1016/0375-9474\(73\)90349-7](https://doi.org/10.1016/0375-9474(73)90349-7)
- Oppenheimer, J. R., & Volkoff, G. M. 1939, *Phys. Rev.*, 55, 374, doi: [10.1103/PhysRev.55.374](https://doi.org/10.1103/PhysRev.55.374)
- Pang, P. T. H., Dietrich, T., Tews, I., & Van Den Broeck, C. 2020, *Phys. Rev. Res.*, 2, 033514, doi: [10.1103/PhysRevResearch.2.033514](https://doi.org/10.1103/PhysRevResearch.2.033514)
- Pang, P. T. H., Tews, I., Coughlin, M. W., et al. 2021, *Astrophys. J.*, 922, 14, doi: [10.3847/1538-4357/ac19ab](https://doi.org/10.3847/1538-4357/ac19ab)
- Postnikov, S., Prakash, M., & Lattimer, J. M. 2010, *Phys. Rev. D*, 82, 024016, doi: [10.1103/PhysRevD.82.024016](https://doi.org/10.1103/PhysRevD.82.024016)
- Rasmussen, C. E., & Williams, C. K. I. 2006, *Gaussian Processes for Machine Learning* (Cambridge, MA: MIT Press)
- Reardon, D. J., et al. 2024, *Astrophys. J. Lett.*, 971, L18, doi: [10.3847/2041-8213/ad614a](https://doi.org/10.3847/2041-8213/ad614a)
- Riley, T. E., et al. 2019, *Astrophys. J. Lett.*, 887, L21, doi: [10.3847/2041-8213/ab481c](https://doi.org/10.3847/2041-8213/ab481c)
- . 2021, *Astrophys. J. Lett.*, 918, L27, doi: [10.3847/2041-8213/ac0a81](https://doi.org/10.3847/2041-8213/ac0a81)
- Saha, A. k., & Mallick, R. 2024, <https://arxiv.org/abs/2410.21877>
- Salmi, T., et al. 2024a, *Astrophys. J.*, 974, 294, doi: [10.3847/1538-4357/ad5f1f](https://doi.org/10.3847/1538-4357/ad5f1f)
- . 2024b, Data and Software for: “The Radius of the High-mass Pulsar PSR J0740+6620 with 3.6 yr of NICER Data”, Zenodo, doi: [10.5281/zenodo.10519473](https://doi.org/10.5281/zenodo.10519473)
- Sieniawska, M., Turczanski, W., Bejger, M., & Zdunik, J. L. 2019, *Astron. Astrophys.*, 622, A174, doi: [10.1051/0004-6361/201833969](https://doi.org/10.1051/0004-6361/201833969)
- Somasundaram, R., Tews, I., & Margueron, J. 2023, *Phys. Rev. C*, 107, 025801, doi: [10.1103/PhysRevC.107.025801](https://doi.org/10.1103/PhysRevC.107.025801)
- Steiner, A. W., Heinke, C. O., Bogdanov, S., et al. 2018, *Mon. Not. Roy. Astron. Soc.*, 476, 421, doi: [10.1093/mnras/sty215](https://doi.org/10.1093/mnras/sty215)
- Steiner, A. W., Lattimer, J. M., & Brown, E. F. 2013, *Astrophys. J. Lett.*, 765, L5, doi: [10.1088/2041-8205/765/1/L5](https://doi.org/10.1088/2041-8205/765/1/L5)
- Takatsy, J., Kovacs, P., Wolf, G., & Schaffner-Bielich, J. 2023, *Phys. Rev. D*, 108, 043002, doi: [10.1103/PhysRevD.108.043002](https://doi.org/10.1103/PhysRevD.108.043002)
- Tan, H., Dore, T., Dexheimer, V., Noronha-Hostler, J., & Yunes, N. 2022, *Phys. Rev. D*, 105, 023018, doi: [10.1103/PhysRevD.105.023018](https://doi.org/10.1103/PhysRevD.105.023018)
- Tang, S.-P., Huang, Y.-J., & Fan, Y.-Z. 2025, *Phys. Rev. D*, 112, 083009, doi: [10.1103/bmsk-8n85](https://doi.org/10.1103/bmsk-8n85)
- Tang, S.-P., Jiang, J.-L., Gao, W.-H., Fan, Y.-Z., & Wei, D.-M. 2021, *Phys. Rev. D*, 103, 063026, doi: [10.1103/PhysRevD.103.063026](https://doi.org/10.1103/PhysRevD.103.063026)
- Tews, I., Krüger, T., Hebeler, K., & Schwenk, A. 2013, *Phys. Rev. Lett.*, 110, 032504, doi: [10.1103/PhysRevLett.110.032504](https://doi.org/10.1103/PhysRevLett.110.032504)
- Thrane, E., & Talbot, C. 2019, *Publ. Astron. Soc. Austral.*, 36, e010, doi: [10.1017/pasa.2019.2](https://doi.org/10.1017/pasa.2019.2)
- Tolman, R. C. 1939, *Phys. Rev.*, 55, 364, doi: [10.1103/PhysRev.55.364](https://doi.org/10.1103/PhysRev.55.364)
- Trotta, R. 2008, *Contemp. Phys.*, 49, 71, doi: [10.1080/00107510802066753](https://doi.org/10.1080/00107510802066753)

- Verma, A., Saha, A. K., & Mallick, R. 2025, *Astrophys. J.*, 985, 1, doi: [10.3847/1538-4357/adcee0](https://doi.org/10.3847/1538-4357/adcee0)
- Vinciguerra, S., et al. 2023, An updated mass-radius analysis of the 2017-2018 NICER data set of PSR J0030+0451, Zenodo, doi: [10.5281/zenodo.8239000](https://doi.org/10.5281/zenodo.8239000)
- . 2024, *Astrophys. J.*, 961, 62, doi: [10.3847/1538-4357/acfb83](https://doi.org/10.3847/1538-4357/acfb83)
- Weih, L. R., Hanauske, M., & Rezzolla, L. 2020, *Phys. Rev. Lett.*, 124, 171103, doi: [10.1103/PhysRevLett.124.171103](https://doi.org/10.1103/PhysRevLett.124.171103)
- Zhou, W., Shen, H., Hu, J., & Zhang, Y. 2024, *Phys. Rev. D*, 110, 043017, doi: [10.1103/PhysRevD.110.043017](https://doi.org/10.1103/PhysRevD.110.043017)